

3.0 REQUIREMENTS FOR AIR QUALITY MODELING SYSTEMS AND DATA ANALYSIS

The data required for this study are primarily driven by the need to drive and evaluate the performance of modeling systems. In evaluating the model performance, the primary concern is replicating the physical and chemical processes associated with actual ozone episodes. This necessitates the collection of suitable emissions, meteorological, and air quality data that pertain to these episodes. This section describes the data requirements of meteorological and air quality models and describes the potential approaches and methods for observation-based data analysis and verification of emission inventories. Recommendations for the CCOS summer 2000 field program are outlined in Section 4.

3.1 Meteorological Modeling

The specification of the meteorological fields that drive the transport and dispersion of atmospheric pollutants is the critical component in mesoscale air quality modeling. The primary objective is to obtain wind fields over the model grid and determine mechanical and convective mixing depths. The simplest way is to use field measurements and interpolate the values over the entire domain. However, field measurements are generally spatially and temporarily sparse, and can be especially inadequate in areas with complex terrain and land-sea interactions. Another way is to use diagnostic and prognostic meteorological models to estimate meteorological fields from existing data and then to adjust these fields through parameterizations of physical processes.

Transport and the dynamics and thermodynamics of the atmospheric boundary layer (ABL) govern dispersion of atmospheric pollutants. The main difficulties in dispersion estimates arise with topographic complexity and increasing atmospheric stability. Turbulence in the ABL is created by wind shear and destroyed by buoyancy and dissipation. Since these effects are nearly balanced in the stable ABL, turbulence intensities are usually low and intermittent. In some cases of stagnant stable conditions the horizontal diffusion of the plume can be of the same magnitude or larger than the actual transport. Moreover, turbulent velocities are frequently affected by gravity waves and the stable ABL undergoes non-stationary evolution. Additional dispersion due to wave phenomena also needs to be resolved. During stable conditions the ABL flow usually decouples from the synoptic winds and the local circulations dominate its flows. In some cases a low-level jet can develop at the top of the surface stable layer and the fate of pollutants at various elevated layers can be completely different over a very small vertical separation. In contrast, during stable and stagnant conditions the winds close to the surface are weak and sometimes below the detection limit of usual instrumentation.

Radiation and advection can also cause fog and cloud formation and significantly change the rate of chemical reactions for some species and deposition processes. The depth of the stable ABL is of the order of 100 m, and radiation processes, as well as local effects such as urban effects, vegetation, soil properties, and small-scale topographic features, can significantly influence ABL characteristics. Plume meandering is frequently observed during stable conditions in topographically complex terrain, and use of data from limited measurement sites can yield erroneous conclusions. All these effects significantly modify transport and dispersion

as well as removal of pollutants. Consequently, an extensive measurement network is necessary in order to capture the spatial and temporal structure of the ABL in a mesoscale domain. The success in any type of dispersion calculation will be limited to appropriate capture and input of atmospheric parameters.

One of the diagnostic models recommended for this study is CALMET. Wind fields in CALMET are calculated in a user specified number of vertical levels by taking into account the influence of terrain on the atmospheric flow and applying an inverse weighting scheme. The initial terrain-adjusted domain mean horizontal components of the wind at each grid point are modified to obtain the final interpolated wind components. CALMET can calculate a spatially variable initial guess field using objective analysis of the measurements. Moreover, CALMET allows use of gridded wind fields created by a prognostic atmospheric model, such as the Penn State University Meteorological Model (MM4, MM5), as “initial guess” fields or as substitutes for observations. CALMET has detailed algorithms for the depth of the convective layer as a function of the potential temperature lapse rate in the layer above the mixing depth, the time step, and the temperature discontinuity at the top of the mixed layer. The daytime mechanical mixing depth is determined from the Coriolis parameter, the friction velocity and the Brunt-Vaisala frequency in the stable layer above the mixed layer. The nighttime depth of mechanical mixing is determined from the friction velocity. CALMET uses an upwind-positioned averaging scheme to smooth out the mixing depths through use of determined weighting factors. Since CALMET has detailed algorithms for wind fields and mixing depth, and furthermore allows initialization with the output from the prognostic atmospheric model, it is an optimum tool for obtaining the initial meteorological fields necessary for estimation of transport, dispersion, and chemical transformation of atmospheric pollutants.

Based on the complexity of terrain in northern and central California, the MM5 model developed by Penn State University and the National Center for Atmospheric Research (NCAR) represents an appropriate tool for resolving dynamics and thermodynamics if used on the scale of 1-2 km horizontal resolution with nesting capabilities. It should include a nonhydrostatic option and full parameterization of physical processes including turbulent transfer. MM5 uses an advanced four-dimensional data assimilation scheme connected to either measurements or synoptic fields. However, uncertainty exists as to the extent to which MM5 can be used to infer turbulence properties in complex terrain. One of the main components in the study is a characterization of the origin and fate of atmospheric pollutants in central California. The main difficulties are due to complex terrain and a number of significant sources within the basin and its surroundings. The results from wind field modeling will be used as input for dispersion and chemical modeling of relevant pollutants also for the entire intensive study period. Atmospheric modeling should treat formation and evolution of fog and clouds, which are essential determinants for liquid-phase chemistry. The detailed information of the three-dimensional plume structure from different sources for the worst case scenarios (highest ground concentrations at the monitoring of interest) will be obtained by wind field, dispersion, and chemical modeling.

The final task is reconciliation of all source apportionment approaches and evaluation of uncertainties, model assumptions, and differences compared to measurements. The main objectives of this task are:

1. Simulate atmospheric processes using MM5 in both fully predictive and data assimilation modes. Since a number of airborne and remote sensing upper-air measurements will be available, it is desirable to place emphasis on the data assimilation mode for the entire field program period. The fully prognostic mode may be desirable for understanding basic characteristics of specific weather episodes with high pollutant concentrations.
2. Determine flow patterns in northern and central California with acceptable horizontal and vertical resolution, using physical parameterization of the main atmospheric processes (radiation, moisture, clouds, and fog).
3. Provide detailed information on the vertical wind and temperature structure of the atmospheric boundary layer during the case studies. Determine elevated layers with specific stability and dynamics. The vertical structure is essential for estimates of transport and dispersion of atmospheric pollutants, as well as for determination of the amount of decoupling of local flows from the air aloft.
4. Determine properties of land-sea breezes, urban circulations, local flows (slope and drainage), and diurnal variation of thermal stability and shear.
5. Determine spatial characteristics of mixing depth for both convective and stable conditions.
6. Estimate properties of turbulence transfer and associated vertical fluxes in the boundary layer.
7. Conduct sensitivity tests of the input parameters (topographic resolution, model grid, synoptic fields vs. radiosonde network, range and variation of sea/surface temperature, urban effects/roughness, sinks and sources of heat).
8. Quantify differences between the predicted and observed wind fields and stability parameters for specific case studies.

The advantages in using a prognostic modeling approach are:

1. High resolution in horizontal and vertical directions.
2. Topography with resolution of 30 seconds embedded within the model structure.
3. Detailed prognostic fields of meteorological parameters (wind, temperature, humidity, turbulence, radiation, clouds).
4. Physically-based estimate of mixing depth in both convective and stable cases, with full spatial and temporal variability.
5. Detailed structure of the small-scale local flows that cannot be resolved through simplified parameterization.

6. Detailed vertical structure of meteorological parameters and stability, which is especially important near sources and receptors and along the transport path.
7. The disadvantages in using a prognostic modeling approach are:
8. The models are fairly complex and expensive to run. Usually they are limited to certain case studies.
9. The models have assumptions in simplification of basic differential equations and numerical techniques and in the parameterizations of physical processes.
10. Integration with dispersion models is usually one of the critical problems.

Nevertheless, atmospheric models are useful tools in understanding the structure and evolution of boundary layer dynamics and providing meteorological fields as input for dispersion models.

3.2 Air Quality Modeling

There are several air quality models that are well established and within the state-of-the-art. The models include CIT, CALGRID, UAM-V, CAMx, CALPUF and EPA's MODELS-3. State-of-the-art air quality models can be applied to simulate photochemical air pollution and aerosol particles. Many of the models can be used to investigate air pollution from urban to regional scales. The models are grid models and some allow two-way nesting so that the model can simulate air pollution on a larger regional scale and on a more highly resolved urban scales simultaneously.

Three different chemical mechanisms are in wide use; carbon bond IV (CBM-IV), SAPRC 1997 and RADM2, all of these mechanisms were validated by extensive testing against environmental chamber data. The chemistry solvers used in the models are relatively fast but more work is needed to make them more general so that it is easier to make changes in the chemical mechanisms. Aerosol formation is not yet understood on a fundamental level. The formation of aerosol particles from the reactions of NO_x, SO₂ and from volatile organic compounds (VOC) are often treated by an empirical thermodynamic approach.

The advection of trace gases has seen some improvement in recent years. There are several possible horizontal advection solvers. The Bott advection solver and the Smolarkiewicz solver are two typical choices. The Bott solver is becoming more popular than the Smolarkiewicz solver because Bott is faster and more accurate with less numerical diffusion than the Smolarkiewicz solver.

The typical files required by an air quality model are shown in Figure 3.2-1. Gridded data files should be available with resolution of at least 1 by 1 km if possible. An air quality model requires files with gridded land use and surface cover over the modeling domain. Typical land use files divide the land use into at least 11 categories (such as urban, rocky, industrial...). A file of the UV surface albedos over the modeling domain is required.

Point, area and biogenic emissions files over the modeling domain are required by the model. Also, files of elevated point sources are required. Gridded emissions files are required for low-level point sources, area and biogenic sources.

3.2.1 Data Requirements for Models

Emissions Inventory

A great amount of care must be taking in preparing the emissions inventory. Without a reasonably accurate emissions it is not possible to accurately model the photochemical formation of ozone and other pollutants. There are two required emissions files; the area source emissions inventory and the elevated point source emissions inventory. Table 3.3-1 shows typical chemicals that need to be included in the emissions inventory. However, the organic chemical emissions should be given in as much detail as possible, rather than just alkane, alkenes etc.

Area source emissions may be considered as part of the boundary conditions (McRae, 1992). The area source file requires that the emissions be given in unites of ppm meter / min. The height of the surface grid box is used to calculate the emissions in unites of ppm / min.

Point sources are assumed to be volume sources in the model filling an entire grid square. Since these are usually hot exhaust stacks, the stack height, diameter, exhaust temperature, flow rate and source strength are needed to calculate the plume rise height and emissions rate.

Air quality files

Air quality files of initial conditions and boundary conditions are required. One of the difficulties of determining the initial conditions is that there are not enough measurements available to determine the three dimensional chemical fields for starting the simulations. It will be necessary to interpolate surface concentrations to estimate vertical distributions. If there are even a few measurements of vertical chemical distributions the relative changes in chemical concentration with height could be used for this interpolation, otherwise typical values for other urban areas will have to be used (Milford et al., 1989). For the boundary conditions it would be desirable to set the boundaries at locations with relatively low emission rates.

Meteorological Files

Typical meteorological data files for air quality modeling are listed in Table 3.3-2.

These fields may be generated through the use of objective analysis of observations or through the use of a meteorological model. The height of the modeling grid must be greater than the mixing height field. The mixing height must be specified relative to the ground surface because the grid follows the local ground elevation. Nighttime conditions for neutral and unstable conditions are directly calculated by the model. The hourly wind components (x, y, z) must satisfy Equation (29) so that the flow fields are mass consistent.

$$\nabla \cdot \mathbf{u} = 0 \quad (29)$$

The rate of chemical reactions is highly dependent upon the temperature. The surface temperature field is used by the chemical solver to determine the correct chemical rate constants. The absolute humidity field is needed by the chemical solver because many reactions, especially the generation and loss of HO_x radicals, are humidity dependent. The solar radiation scaling field is needed to calculate the atmospheric stability. The ultraviolet radiation scaling field is required to calculate photolysis rates. Both the solar radiation scaling field and ultraviolet radiation scaling field are affected by the presence of clouds and this effect should be incorporated into the data files for these quantities.

In order to determine the aerodynamic surface roughness, surface resistances and deposition velocities land use, it is necessary to specify the land use for each grid square. Typical land use categories include high rise urban, residential, deciduous forestland and evergreen forest categories. Files for the orography of the domain are also required.

3.3 Review of previous SAQM studies and implications for CCOS measurement sites.

The SAQM modeling results for central California finds maximum ozone concentrations near 120 ppb. The maximum ozone concentrations occur along a line running from the San Francisco Bay Area through Sacramento to the front range and along the San Joaquin valley. For example Figure 3.3-1 shows a plot of ozone concentrations over central California at noon on the second simulated day. The area directly west of the San Francisco Bay Area has ozone concentrations near 120 ppb while high ozone concentrations are found along and directly west of the San Joaquin valley. The surface ozone concentrations show strong diurnal variation. Figure 3.3-2 shows that at midnight the ozone concentrations drop to near 40 ppb or less at the western boundary and over the San Joaquin Valley.

To be able to measure these changes in ozone to test the models it is necessary to have measurement stations along the line running from the San Francisco Bay Area through Sacramento to the front range and along the San Joaquin valley. The model predicts that ozone concentrations show strong variations over this region due to transport, deposition and chemistry. Measurement stations to measure ozone concentrations and the concentrations of precursors and other photochemical products placed along the west – east line will help to determine if the models represent a scientifically reasonable description of ozone formation and transport. The same can be said of an array of measurements through the San Joaquin valley.

It is also important to have measurement stations to the north and south of the Sacramento area because in this area there are often meteorological situations where the wind fields from the west diverge toward the north and south. The ozone concentrations shown in Figure 3.3-3 shows several ozone hot spots one directly east of the San Francisco Bay Area with two more directly to the north and south. Measurements to the north and south in this area will help determine if the model predicted patterns are real. Figure 3.3-3 also shows high ozone concentrations along and directly east and south of the San Joaquin valley. Measurement stations are required at this sites as well.

The SAQM model predicts a rather complex vertical structure in ozone concentrations, Figure 3.3-4. In the simulations that were analyzed here the vertical structure along a north – south cross section through the center of central California near Sacramento was especially interesting. In Figure 3.3-4 the vertical coordinate is linear in pressure following coordinates and this exaggerates the apparent height. At noon on the second day the ozone concentrations in the Sacramento area are very high. The model calculates that ozone is lost and transported to the north and south leaving an arc of ozone that extends aloft and to the east and west by midnight. Ozone sondes and possibly LIDAR measurements would be very helpful in the observation of this complex vertical structure. It should be positioned to observe the diurnal variations to the north and south of Sacramento.

The vertical structure of the ozone concentrations the west – east cross section through central California along the line running from the San Francisco Bay Area through Sacramento to the front range is similar in its overall behavior to the north – south line, Figure 3.3-5. The plots show evidence of transport of ozone and NO_x from the west to the east. Ozone is lost in the lower levels and remains relatively high aloft as the time progresses from noon to midnight. Some of the parcels of high ozone are seen to travel from west to east in this sequence. Ozone sondes near the San Francisco and Sacramento and aircraft measurements of ozone over the front range and the western boundary are required to observe this complex ozone structure predicted by the models.

Some measurements of NO_x , formaldehyde and other VOCs need to be made at the western boundary to better define the boundary conditions for modeling. In the SAQM simulations that we examined the western boundary generated 5 ppb of HCHO, Figure 3.3-6. These high HCHO concentrations are a potential problem since HCHO is extremely reactive in producing ozone. The same is true for NO_x concentrations. Figure 3.3-7 shows that the western boundary has over 0.5 ppb of NO. These moderate NO concentrations over the ocean appear to be due to transport from the model's boundary. More measurements to better define the boundary conditions, especially at the western boundary are required to constrain the modeling activities.

3.4 Emissions Characterization

Point source emissions occur at facilities that can be identified by name and location and emit more than the threshold value specified by the local air pollution control district (APCD). A facility may have many individual identifiable sources (points) of emissions, and a point source may correspond to one or more processes or operations. Point-source activity levels usually relate to a process rate. Emission factors are derived from tests that relate emissions to the process causing the emissions. Point source emission estimates are based primarily upon data collected by the county APCDs and air quality management districts (AQMDs). Point source emission estimates are stored and maintained in the California Emission Inventory Development and Reporting System (CEIDARS), and are also reported to the national Aerometric Information Retrieval System (AIRS), which is maintained by the U.S. Environmental Protection Agency.

Most area sources are small emitters that are not accounted for in the point source portion of the CEIDARS database. Some examples of area sources are residential space heaters,

agricultural burning, pesticide applications, and consumer products. Area source emission estimates are developed by the districts and by the ARB staff. Area source methods are used to estimate emissions for approximately 260 emission source categories in the emission inventory. These categories, which include both stationary and other mobile sources, are divided into four types of emission sources. Aggregated point sources are many small point sources, or facilities, that are not inventoried individually but are estimated as a group and reported as a single source category. Examples include gas stations and dry cleaners. Area-wide sources include source categories associated with human activity and emissions take place over a wide geographic area. Consumer products and agricultural operations are examples of area-wide sources. Non-anthropogenic sources generally include source categories with naturally occurring emissions such as geogenic sources and wildfires. Other mobile sources include categories such as farm equipment and off-road recreational vehicles. Collectively, these types of sources are referred to as area source categories. The ARB staff is responsible for 130 area source categories. The air pollution control and air quality management districts are responsible for the remaining categories.

The Mobile Source Control Division of the ARB has primary responsibility for developing on-road and off-road mobile source emission factors in California. The ARB Office of Air Quality and Transportation Planning has the responsibility for developing the motor vehicle activity components such as vehicle-miles-traveled, starts, and vehicle population, which are used by the models. Emission factors developed for passenger car, light, medium and heavy-duty vehicles are used to develop models predicting the emissions for all on-road motor vehicles.

On-road mobile sources are motor vehicles that travel on public roads. This category consists of gasoline-powered and diesel-powered passenger cars, light-duty trucks (6,000 lbs. gross vehicle weight [GVW] or less), medium-duty trucks (6,001-8,500 lbs. GVW), heavy-duty trucks (over 8,500 lbs. GVW), urban buses, and motorcycles. Emissions from motor vehicles include exhaust, evaporative, crankcase, and tire-wear emissions. Four computer programs (CALIMFAC, WEIGHT7n, EMFAC7n, and BURDEN7n) are used to produce the motor vehicle emission inventories. These models are described in detail by the ARB (1996). Model versions are indicated by the letter “n”. The current version, EMFAC 7G, was released in 1996. The CALifornia Inspection/Maintenance emission FACTor” (CALIMFAC) program computes base emission rates for each technology group with and without inspection and maintenance (I/M) benefits. The base emission rates consist of a zero mile rate and a deterioration rate for each model year for each pollutant. The “EMission FACTor” (EMFAC) model computes fleet composite emission factors by vehicle class and technology for a calendar year. The WEIGHT program provides EMFAC with activity weighting fractions for individual model years so that composite emission factors can be produced. WEIGHT also provides the accumulated mileage by model year for any particular calendar year in order to calculate the “deteriorated” emission rate for a model year. BURDEN calculates the emission estimates in tons/day by multiplying the composite emission factors from EMFAC by activity factors. Vehicle miles traveled, vehicle type distribution, and trip lengths, the input data for BURDEN are obtained from the California Department of Motor Vehicles (DMV) and the California Department of Transportation. BURDEN adjusts emission rates according to speed, ambient temperature, and heavy-duty I/M benefits.

Motor vehicle emission rates consist of running, incremental cold start, and incremental hot start exhaust emissions for TOG, CO, and NOx, and hot soak, diurnal, running and resting evaporative emissions for TOG. Running exhaust emissions include emissions from the tailpipe or through the crankcase after the vehicle is warmed up and in a stabilized mode. Running exhaust emissions also include exhaust particulate matter and particulate matter from tire wear. Cold start emissions occur from the time the engine starts, after being off for one or more hours for a catalyst-equipped vehicle and four or more hours for a non-catalyst-equipped vehicle, until the coolant achieves its nominal operating temperature. Cold start emissions are incremental emissions that are added to the running emissions. The hot start mode occurs after a short engine-off period, less than one hour for a catalyst-equipped vehicle and less than four hours for a non-catalyst-equipped vehicle. Hot start emissions are also incremental to running emissions. Hot soak emissions result from gasoline vaporization from elevated engine and exhaust temperatures after the engine is turned off at the end of a trip. All of these emissions are assumed to be proportional to average vehicle miles traveled. The emission rates for hot soak emissions are expressed as grams of TOG per trip rather than as grams of TOG per vehicle mile traveled (VMT). Diurnal evaporative emissions result from the daily changes in the ambient temperature due to expansion of the air-fuel mixture in a partially filled fuel tank. Running evaporative losses are releases of gasoline vapor from the fuel system during vehicle operation (included for the first time in EMFAC7E). Resting loss evaporative emissions are due to fuel line hose or fuel tank permeation (included for the first time in EMFAC7F).

Three types of inventories are available from the ARB: daily average, planning, and gridded. The average daily emissions are expressed as an emission rate in tons per average day, determined by dividing annual emissions by 365. Countywide and basinwide totals are provided by source categories. This inventory is updated and published annually by the ARB. BURDEN can produce planning inventories that take into account the effects of diurnal and seasonal variations in temperature and activity patterns. The planning inventories provide emission estimates for six periods (0000-0600, 0600-0900, 0900-1200, 1200-1500, 1500-1800, and 1800-2400 PST or PDT) during an average summer and winter day.

The Direct Travel Impact Model (DTIM) assigns emission rates to locations and time periods to provide input to air quality models. DTIM is BURDEN's analog for gridded inventories. DTIM was developed jointly by Caltrans and the ARB. DTIM uses the temporal and spatial distributions of motor vehicle activities provided by a travel demand model, the summarized composite vehicle emission rate from EMFAC, and an input file of parameters such as hourly temperatures by grid cell to calculate and distribute emissions into the grid system defined by the user.

Emission backcasts and forecasts are made by the ARB using base year emissions in conjunction with estimates of growth and emission control effectiveness. Emission growth is based upon available projections of socio-economic trends. Emission reductions are based upon adopted regulations and control measures. Backcast and forecasts are also available for planning inventories.

3.5 CCOS Emission Inventory Development

A technical committee has been established to develop and oversee emission inventory development projects that may be conducted in support of CCOS. The group consists of ARB emission inventory branch and the air pollution control districts in the study area. The following projects are currently under consideration.

1. Collection and analysis of day-specific traffic count information for the CCOS modeling domain.
2. Integration of transportation data for CCOS domain, resolve transportation model differences, and run DTIM for entire modeling domain.
3. Collection of day-specific emission data for wildfires, controlled burns, and agricultural burns.
4. Develop base and future year gridding surrogates for spatial distribution of stationary area source emission categories.
5. Development of point and area source emission inventories for small districts.
6. Expansion of biogenic emission model to CCOS domain.
7. Emission Inventory Validation Studies

3.6 Evaluation of Emission Inventory Estimates

Uncertainties in precursor emissions are largely viewed as one of the weaker links in the air quality modeling process. Independent evaluations of emission inventory estimates must be an integral component of air quality modeling studies. Approaches for evaluation of emission inventories include: 1) performance evaluations of air quality simulation models; 2) source apportionment by receptor modeling; 3) spatial and temporal comparisons of ambient and emission inventory non-methane organic gas speciation profiles and pollutant ratios (e.g., CO/NO_x and VOC/NO_x); 4) comparisons of long-term trends in ambient pollutant concentrations and concentration ratios with emission inventory trends; 5) comparisons of on-road measurements with motor vehicle emission models; and 6) fuel-based inventory based on regional gasoline sales and fleet-averaged, fuel-based emission factors from remote sensing measurements.

3.6.1 Compare Proportions of Species

Comparisons of the ambient pollutant ratios with corresponding ratios derived from emission inventory estimates have been widely used to determine consistency between emission inventory estimates and ambient measurements. This approach has been used in the Southern California Air Quality Study (Fujita et al., 1992), the San Joaquin Valley Air Quality Study (Fujita et al., 1994), the Lake Michigan Ozone Study (Korc et al., 1993) and by the ARB in response to requirements of SB 2174 (ARB, 1997). The premise of this evaluation approach is that in areas with high emission rates, early morning NMOG/NO_x and CO/NO_x ratios and

speciation profiles in emission estimates should compare well with observed ambient ratios and speciation profiles for the same time period. Issues that are important to address in this type of comparison include: 1) the importance of ground level versus elevated plumes and their influence on ground level measurements; 2) the location of ambient monitoring sites (at urban locations, nearly all sites are located adjacent to roadways); 3) pollution carry-over from the previous day(s); 4) the reliance upon NO_x as the reference species for the "top-down" ratio comparison, including the assumption that NO_x emissions are reasonably accurate; 5) hydrocarbon speciation differences between ambient data and the inventory; and 6) representativeness of the monitoring site in characterizing a grid cell's emissions and ambient concentrations.

3.6.2 Source Apportionment by Chemical Mass Balance Receptor Modeling

The Chemical Mass Balance (CMB) model (Friedlander, 1973; Cooper and Watson, 1980; Gordon, 1980, 1988; Watson, 1984; Watson et al., 1984; 1990; 1991; Hidy and Venkataraman, 1996) consists of a least-squares solution to a set of linear equations which expresses each receptor concentration of a chemical species as a linear sum of products of source profile species and source contributions. The source profile species (the fractional amount of the species in the NMOG emissions from each source type) and the receptor concentrations, each with uncertainty estimates, serve as input data to the CMB model. The output consists of the contributions for each source type to the total ambient NMOG as well as to individual NMOG concentrations. The model calculates values for contributions from each source and the uncertainties of those values. Input data uncertainties are used both to weight the relative importance of the input data to the model solution and to estimate uncertainties of the source contributions. CMB software currently in use (Watson et al., 1990) applies the effective variance solution developed and tested by Watson et al. (1984) because: 1) it calculates realistic uncertainties of source contributions from both the source and receptor uncertainties; and 2) chemical species measured more precisely in both source and receptor samples are given greater influence in the solution than are less precisely measured species. The software also incorporates collinearity measures (Henry, 1982, 1992) to assess the effects of source profile similarity on source contribution estimates and their standard errors. The software is interactive, allowing many sensitivity and assumptions-testing sets to be performed rapidly.

In addition to developing the CMB software, DRI investigators have developed and formalized the protocol for applying and validating the CMB model (Pace and Watson, 1987; Watson et al., 1991; 1998) for apportioning particles (Watson et al., 1994) and gaseous organic compounds (Fujita et al., 1994). In the past six years, DRI investigators have applied the CMB receptor model to PAMS or PAMS-type speciated NMOG data from southern California (Fujita et al., 1994), San Joaquin Valley, CA (Fujita et al., 1995a), southeast Texas (Fujita et al., 1995b), northeastern U.S. (Fujita and Lu, 1998a), Phoenix, AZ (Fujita and Lu, 1997a), western Washington (Fujita et al., 1997b), El Paso, TX (Fujita, 1998), and Austin, TX (Fujita et al., 1999).

The application of continuous speciated VOC data in source apportionment offers additional insights regarding the temporal variations in source contributions that are difficult to discern from a limited number of canister samples that are integrated over a period of 3 hours or

more. The following graphical display show examples of CMB results obtained from hourly speciated hydrocarbon data.

- Average source contribution estimates of ambient hydrocarbons by hour of day (e.g., Figure 3.5-1)
- Diurnal plots of the average CMB source contribution estimates by site for each day of the week (e.g., Figure 3.5-2).
- CMB source contributions and residual hydrocarbon concentrations and graphical displays of residuals by wind direction and time of day (e.g., Figure 3.5-3).

Another useful graphical display that can also be applied to time-integrated canister samples show relationships between source contribution estimates (in particular the residual unexplained mass) and extent of reaction of the ambient air sample (estimated by a ratio of reactive to unreactive hydrocarbon species. Scatterplots of CMB-predicted versus measured concentrations for reactive species by site and time of day are also useful in examining the photochemical age of the ambient hydrocarbons.

For CCOS, we propose comparing the ambient source apportionment at selected measurement sites with a model and emission inventory based CMB analysis. A dispersion model could be used to estimate the concentrations of the various species at measurement sites based upon the meteorology and emission inventory. This calculation should be made for specific chemical species and not lumped species. First order loss chemistry based upon rate constants and concentrations of HO and O₃ could be included in the dispersion models for each reactive VOC. The HO concentrations would be calculated from 3-d model such as CAMx. The dispersion model estimated concentrations at a specific measurement site would be subjected to CMB analysis. Comparison of the observed source apportionment with the model derived source apportionment will provide an excellent test of the emission inventory. Comparison of the model derived source profiles with and without chemistry should provide a useful check of the CMB approach. Specifically compare ozone precursor, NO_x, CO and VOC on a diurnal and weekday basis as estimated by model with the measurements should also be included.

3.6.3 Remote Sensing of Vehicle Exhaust Emissions and Fuel-Based Inventories

With initial support from the Colorado Office of Energy Conservation in 1987, the University of Denver (DU) developed an infra-red (IR) remote monitoring system for automobile CO exhaust emissions. The current instrument measures CO, HC, NO and smoke opacity. The additional capability to simultaneously monitor aromatic hydrocarbons and low molecular weight aldehydes is currently under development. The remote sensing detector (RSD) has been widely used to identify high-emitting vehicles and to characterize the emissions distributions for large fleets of on-road motor vehicles.

The instrument was designed to emulate the results one would obtain using a conventional non-dispersive infra-red (NDIR) exhaust gas analyzer. Thus, the RSD is also based on NDIR (NDUV for NO). An interference filter that transmits infra-red (IR) light of a wavelength known to be absorbed by the molecule of interest is placed in front of a detector.

Reduction in the signal caused by absorption of light by the molecules of interest produces a reduction in the detector's voltage output. One way of conceptualizing the instrument is to imagine a typical garage exhaust NDIR instrument in which the separation of the IR source and detector is increased from 10 cm to 20-40 feet. Instead of pumping exhaust gas through a flow cell, a car now drives between source and detector. The light source, across the road, now contains a deuterium lamp, which is mounted in such a manner that the net result from the source is a collimated beam of UV and IR light. Because the effective plume path length and amount of plume seen depends on turbulence and wind, one can only look at ratios of CO, HC, or NO to CO₂. These ratios are termed Q for CO/CO₂, Q' for HC/CO₂, and Q'' for NO/CO₂ and are constant for a given exhaust plume. By themselves, Q and Q' are useful parameters with which to describe the combustion system.

With the aid of a fundamental knowledge of combustion chemistry, many parameters of the vehicle's operating characteristics can be determined including the instantaneous air/fuel ratio, the %CO, %HC, or %NO which would be read by a tailpipe probe, and the grams CO, HC, or NO emitted per gallon of gasoline (gCO/gallon or gHC/gallon) emissions (Bishop and Stedman 1996). The following formulas assume a fuel density of 750 g/L and 0.86 g carbon per gram of fuel (Stedman 1998).

$$\text{gCO/gal} = 5671 * Q / (1 + Q + 3*Q')$$

$$\text{gHC/gal} = 8911 * Q' / (1 + Q + 3*Q')$$

$$\text{gNO/gal} = 6076 * Q'' / (1 + Q + 3*Q')$$

Remote sensing has been shown to give accurate readings for CO by means of double-blind studies of vehicles both on the road and on dynamometers (Lawson et al., 1990; Stedman and Bishop, 1990). EPA has shown that the readings are closely comparable to laboratory readings from a vehicle on a dynamometer (Stedman and Bishop, 1990). Lawson and coworkers used a vehicle with variable emissions under passenger control to show the correctness of the on-road readings (Lawson et al., 1990). Independent studies (Ashbaugh et al., 1992) show that the CO readings are correct within $\pm 5\%$ and HC within $\pm 15\%$. Recent work (Stedman et al., 1997) has shown that fleet average on-road emissions by model year correlate with IM240 readings with r^2 greater than 0.95 for CO, HC and NO.

The fact that remote on-road readings are well correlated with more complex tests is also illustrated by a study in California (CARB, 1994 and Knapp 1992) in which the remote sensing readings were used in California immediately to pull over apparently gross polluting vehicles which were then tested by a team of Smog-Check engineers, and then brought to a dynamometer and subjected to the EPA IM240 test. Of 79 vehicles tested on IM240, 76 failed and the three which passed had all failed the previous Smog-Check.

The remote sensor is accompanied by a video system when vehicle identification information is required. The video camera is coupled directly into the data analysis computer so that the image of each passing vehicle is frozen onto the video screen. The computer writes the date, time, and the CO, NO, HC and CO₂ concentrations at the bottom of the image. These images are then stored on videotape. The digital database also contains uncertainty limits and

opacity data. The height of the sensing beam is typically set at 20-30 cm above the road surface optimally to observe exhaust plumes from light duty vehicles, including gasoline and diesel-powered vehicles, as long as the exhaust plume exits the vehicle within a few feet of the ground.

The remote sensor is effective across single or multiple traffic lanes of up to 40 feet in width. However, if one wishes to positively identify and video each vehicle with its exhaust, it is optimally efficient when used across a single lane of traffic. FEAT operates most effectively on dry pavement. Rain, snow, and vehicle spray from very wet pavement cause interferences with the optical beam. These interferences do not cause incorrect readings, rather they cause the frequency of invalid readings to increase, ultimately to the point that all data are rejected as being contaminated by too much "noise". At suitable locations exhaust can be monitored from over one thousand vehicles per hour.

3.7 Observation-Driven Methods

Observation-based approaches use high-quality ambient measurements of O₃, its precursors, and/or secondary products of the photochemical mechanism to diagnose the underlying relationship between O₃ production and sources of O₃ precursors. The methods range from those that rely solely on analysis of chemical measurements to more complex methods that rely on photochemical models as well as observations to diagnose VOC- or NO_x-limitation.

The following are four such methods.

1. The correlation between ozone and NO_y or NO_z (e.g., Trainer et al., 1993; Jacob et al., 1995)
2. The Integrated Empirical Rate (IER) model of Johnson (1984), as revised by Blanchard et al., (1994) and Chang et al., (1995). Method is also known as Smog Production (SP) algorithms.
3. The use of indicator species and ratios (e.g., NO_y, NO_z, O₃/NO_y, O₃/HNO₃, HCHO/NO_y, H₂O₂/HNO₃, H₂O₂/NO_y, and H₂O₂/NO_z) (Sillman et al., 1990; Milford et al., 1994; Sillman, 1995; Watkins et al., 1995; Jacob et al., 1995), and
4. The observation-based model (OBM) of Cardelino and Chameides (1995).

Observation-based methods provide procedures for deriving O₃ precursor relationships that are independent of emission inventories and other inherently uncertain inputs. However, these methods are not without their own limitations and uncertainties, and are best used in conjunction with air quality simulation models.

3.8 Contribution of Transported Pollutants to Ozone Violations in Downwind Areas

Although past transport studies have documented pollutant transport on specific days, they have not always quantified the contribution of transported pollutants to ozone violations in the downwind area. Quantitative estimates of the contribution of transported pollutants to ozone violations in the downwind area can be accomplished by photochemical grid modeling and by

advanced data analysis techniques such as “flux planes” measured by aircraft which traverse a vertical plane perpendicular to a suspected transport corridor at different elevations.

In principle, well-performing grid models have the ability to quantify transport contributions. However, many of the interbasin transport problems involve complex flow patterns with strong terrain influences that are difficult and expensive to model. Upper-air meteorological and air quality data in critical transport locations is generally required in order to properly evaluate and use grid models for quantifying transport contributions. In combination with modeling, data analyses can improve the evaluation of modeling results and provide additional quantification of transport contributions.

In order to quantify pollutant transport and to provide data for modeling and data analyses, surface and aloft measurements are needed at locations where transport can occur and at the times when transport is occurring. These monitoring locations include in and near mountain passes, along coastlines, offshore, and at various locations in the downwind air basin.

Previous studies (e.g., Roberts et al., 1993) have used aircraft measurements to calculate transport across flux planes. Vertical planes, intersecting the profiler sites downwind of and perpendicular to the transport path, can be defined and provide estimates of transport through these passes using surface and aircraft measurements of pollutant concentrations and surface and wind profiler data for volume flux estimations.

3.9 Contributions of Elevated NO_x Sources to Downwind O₃

Power plants and other sources with tall stacks are significant sources of NO_x, which in the presence of NMHC can lead to catalytic formation of ozone downwind of the source. However, close to the stack there is a temporary decrease in ozone levels due to “titration” by high levels of NO in the near field of the plume. Further downstream, ozone levels above the local background indicate net ozone production due to the reaction of plume NO_x with NMHC that are entrained into the plume in the dilution process. However, questions remain as to how much ozone is actually produced in the plume, how the ozone production efficiency depends on the chemical composition of the plume, and what the relative contributions of power plants are to high ozone episodes in downwind areas.

Recent power plant plume studies (Senff et al., 1998) utilized airborne ozone and aerosol lidar in conjunction with other instrumented aircraft. Because of its ability to characterize the two dimensional structure of ozone and aerosols below the aircraft, the airborne lidar is well suited to document the evolution of the size and shape of the power plant plume as well as its impact on ozone concentration levels as the plume is advected downwind.

3.10 Deposition Studies

During the California Ozone Deposition Experiment (CODE) in 1991, aircraft and tower-based flux measurements were taken over different types of San Joaquin crops, irrigated and non-irrigated fields, and over dry grass. Results are briefly summarized in Pun et al. (1998) and include estimates of ozone deposition velocities of 0.7-1.0 cm/s (Pederson et al. 1995). Vertical fluxes (deposition rates) can be calculated if a vertical gradient is known (assumed or measured).

Order of magnitude calculations by Pun et al. show that dry deposition can be a few percent (~3-5%) of the total ozone budget in the San Joaquin Valley.

Reasons for further flux and deposition measurements during the CCOS study, with its expanded geographic scope, are at least three-fold:

1. Further consideration of NO sources. While NO was not considered to be a problem at three sites reported on by Pederson et al. (1995), Mahrt et al. (1995) found that rapid titration of O₃ by NO did affect aircraft-based flux O₃ surface flux measurements. Controlled experiments that employ a spatially diverse array of NO_x monitors upwind or surrounding a flux measurement site could help quantify this effect.
2. Further consideration of relative humidity effects. The Sacramento River Delta region and coastal regions are part of the CCOS domain. Ozone is not highly water soluble, but McLaughlin and Taylor (1981) report that ozone deposition to plants can increase by a factor of 2-3 when relative humidity changes from 35% to 75%. Based on this, Mahrt et al. (1995) suggest that ozone deposition may show a more complex spatial and/or temporal pattern than heat and moisture fluxes. Deposition studies for CCOS could include measurement of ozone fluxes over more varied types of terrain within the CCOS study area, including the higher humidity areas of delta or the coastal areas. Desjardins et al. (1995) report that aircraft flux measurements compared well with tower-based flux measurement at two instrumented vineyard sites during CODE. Aircraft could be used to expand the diversity of sites measured.
3. Precursor deposition rates. Fluxes of NO_x and VOC were not measured during CODE.

Table 3.3-1. Typical chemical species in an emission inventory for modeling.

| | |
|-----|------------------------------------|
| 1. | Nitrogen dioxide |
| 2. | Nitric oxide |
| 3. | Sulfur dioxide |
| 4. | Carbon monoxide |
| 5. | Methane |
| 6. | Ethane |
| 7. | Higher alkanes |
| 8. | Ethene |
| 9. | Terminal alkenes |
| 10. | Internal alkenes |
| 11. | Isoprene |
| 12. | Benzene |
| 13. | Toluene |
| 14. | Xylene and more reactive aromatics |
| 15. | Carbonyls |
| 16. | Formaldehyde |
| 17. | Acetaldehyde and higher aldehydes |
| 18. | Ketones |

Table 3.3-2. Required meteorological files.

| |
|-------------------------------------|
| Mixing depth field |
| Three dimensional wind field |
| Surface temperature field |
| Absolute humidity field |
| Solar radiation scaling field |
| Ultraviolet radiation scaling field |

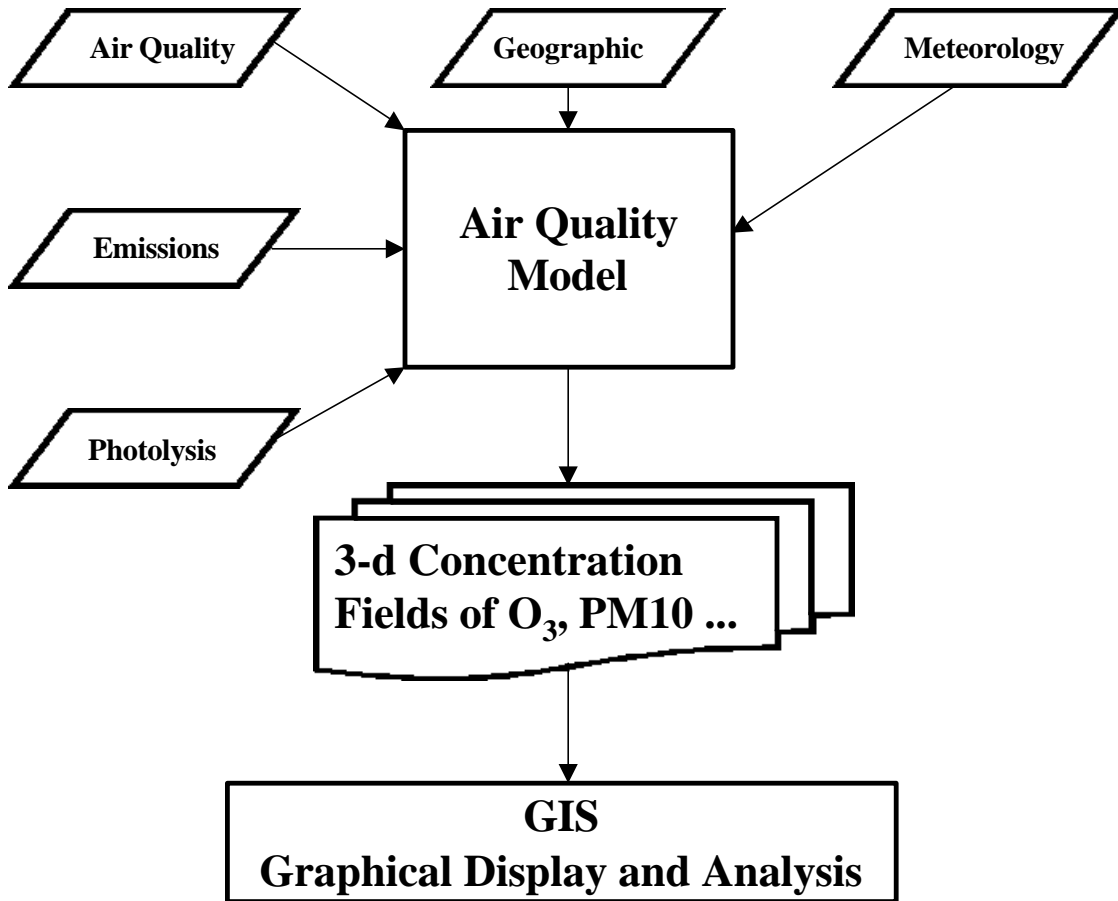


Figure 3.2-1. File typically required by photochemical air quality model.

Figure 3.3-1. Plot of ozone concentrations over central California at noon on the second simulated day. The area directly west of the San Francisco Bay Area has ozone concentrations near 120 ppb while high ozone concentrations are found along and directly west of the San Joaquin valley.

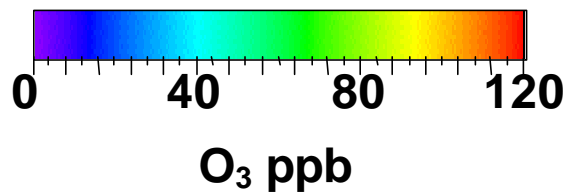
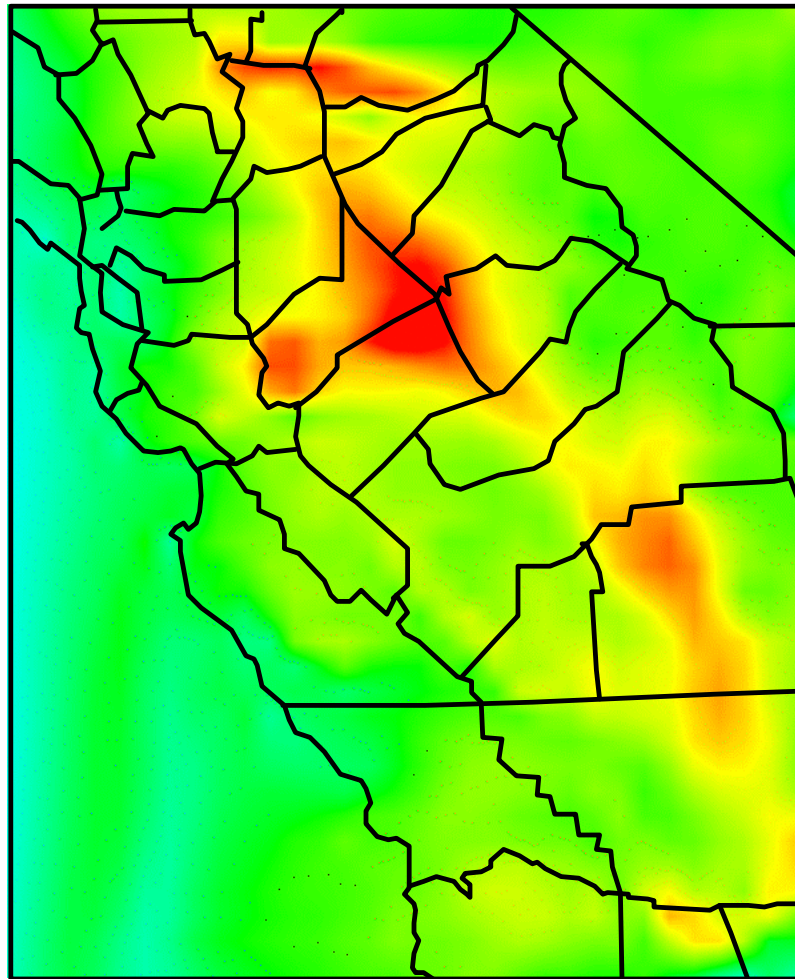


Figure 3.3-2. Plot of ozone concentrations in central California at midnight after two simulated days. Note that the western boundary and the San Joaquin Valley have ozone concentrations near 40 ppb or less.

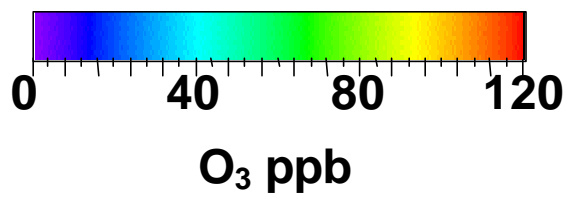
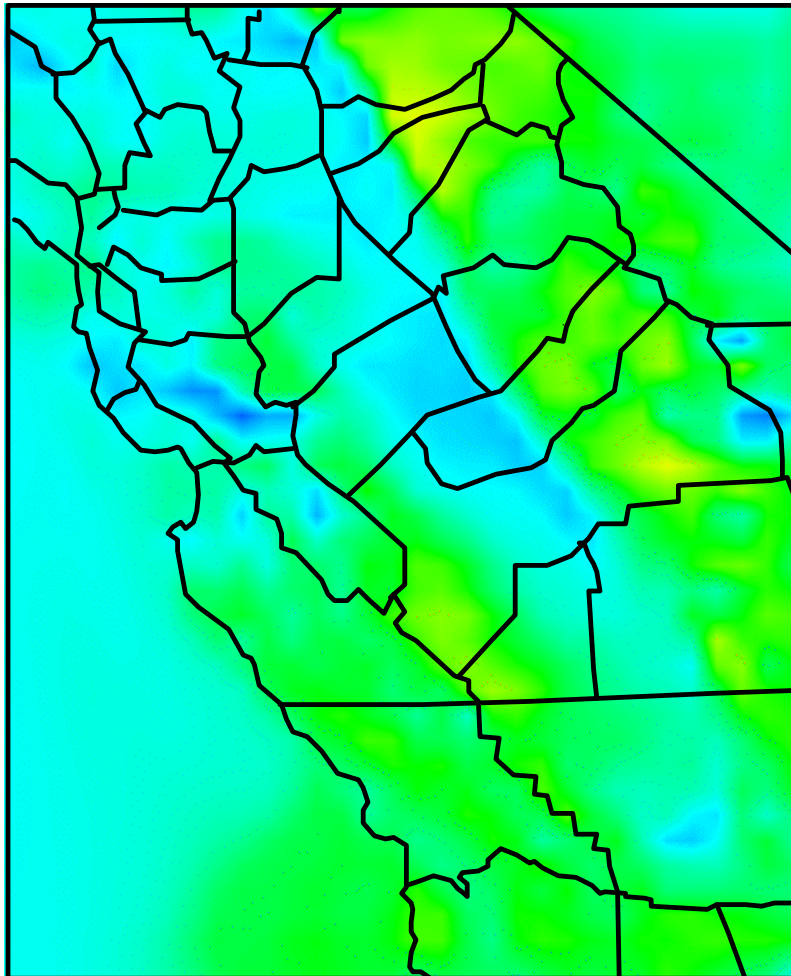


Figure 3.3-3. Plot of ozone concentrations in central California at noon on the third simulated day. The high ozone pattern is more complicated with several ozone hot spots one directly west of the San Francisco Bay Area with two more directly to the north and south. High ozone concentrations are found also along and directly west and south of the San Joaquin valley.

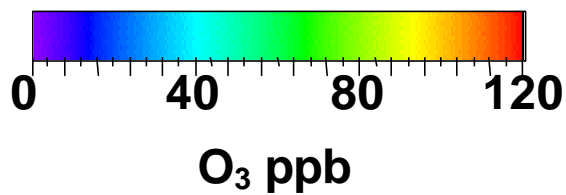
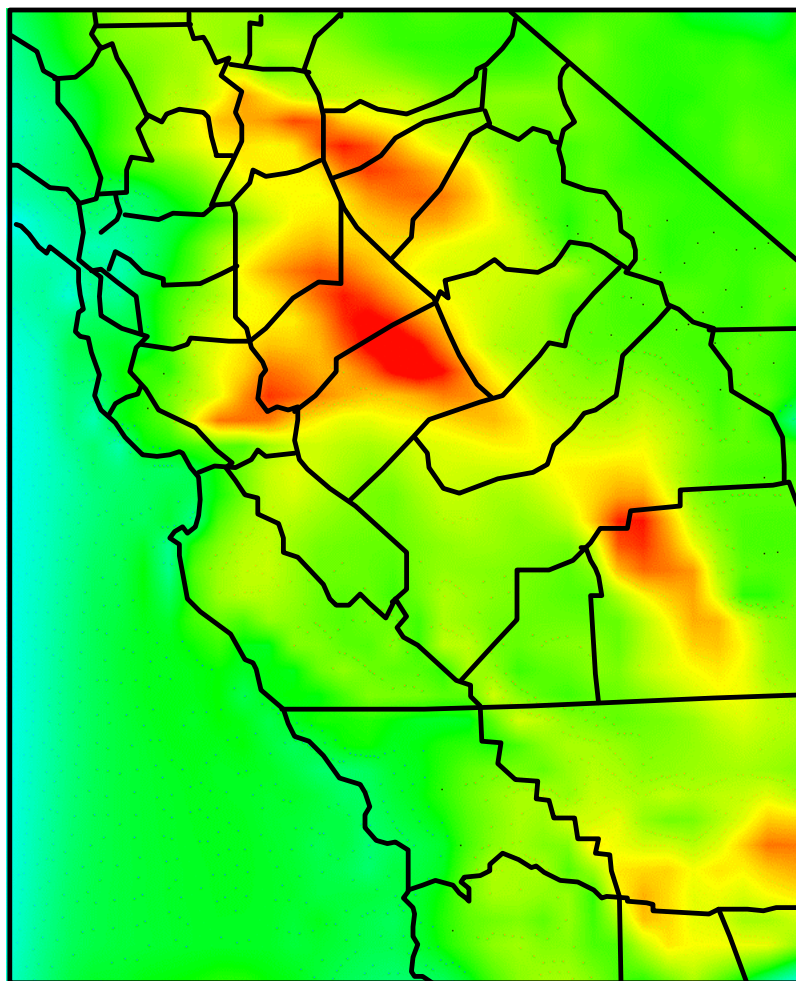


Figure 3.3-4. Plot of ozone concentrations in the vertical along a north – south cross section through the center of central California. The vertical coordinate is linear in pressure following coordinates which exaggerates the apparent height. Plot A shows the ozone concentrations at noon on the second day and Plot B shows the ozone concentrations at midnight after two simulated days. The high ozone concentrations at noon, Plot A, and the low ozone concentrations at midnight, Plot B, are found over the Sacramento area.

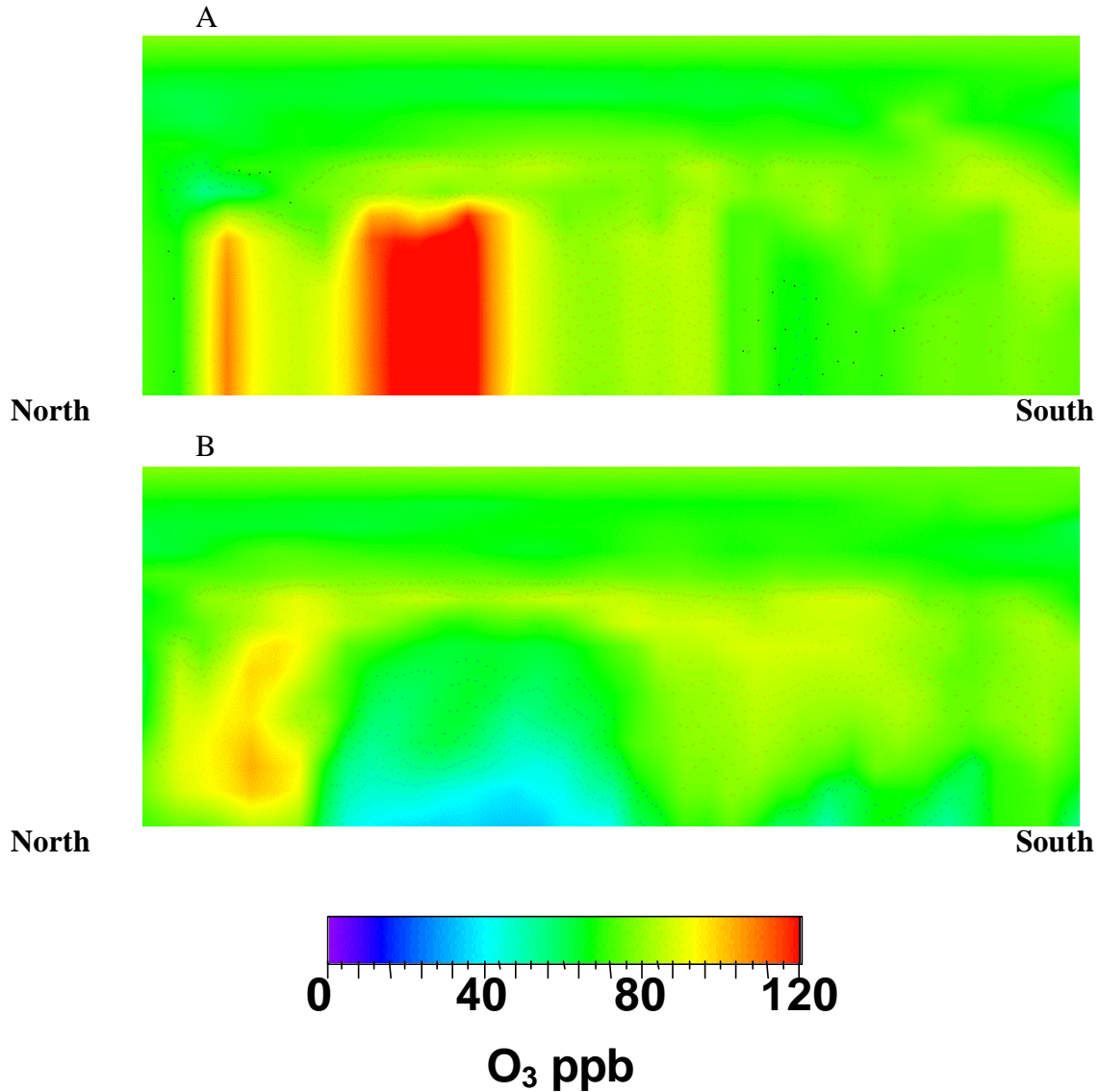


Figure 3.3-5. Plot of ozone concentrations in the vertical along a west – east cross section through central California along a line running from the San Francisco Bay Area through Sacramento to the front range. The vertical coordinate is linear in pressure following coordinates which exaggerates the apparent height. Plot A shows the ozone concentrations at noon on the second day, Plot B shows them at 6:00 PM on the second day and Plot C shows them at midnight after two simulated days. The plots show evidence of transport of ozone and NO_x from the west to the east.

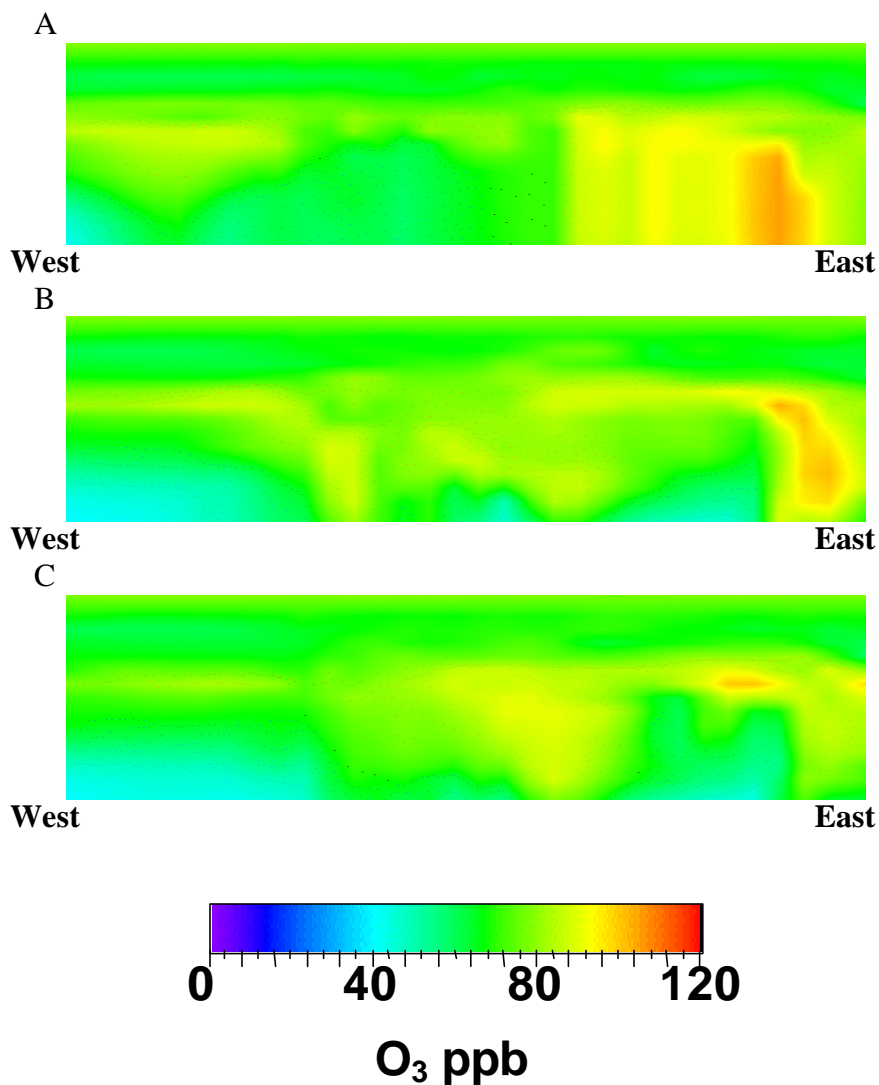
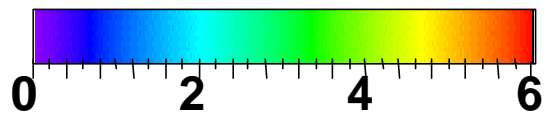
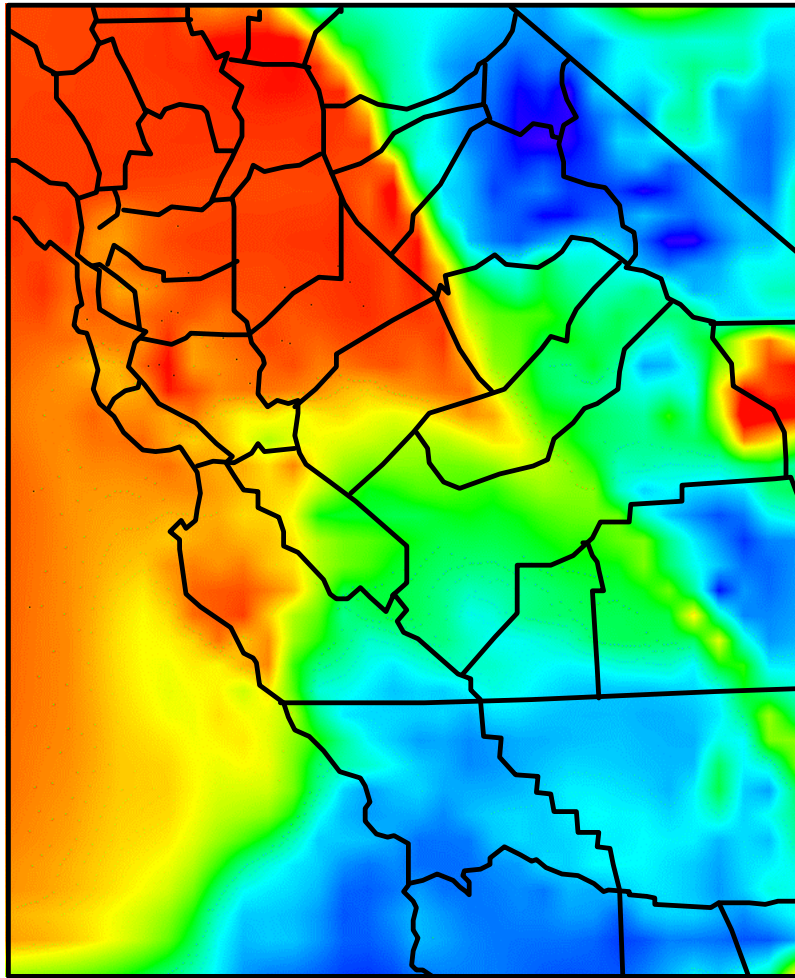
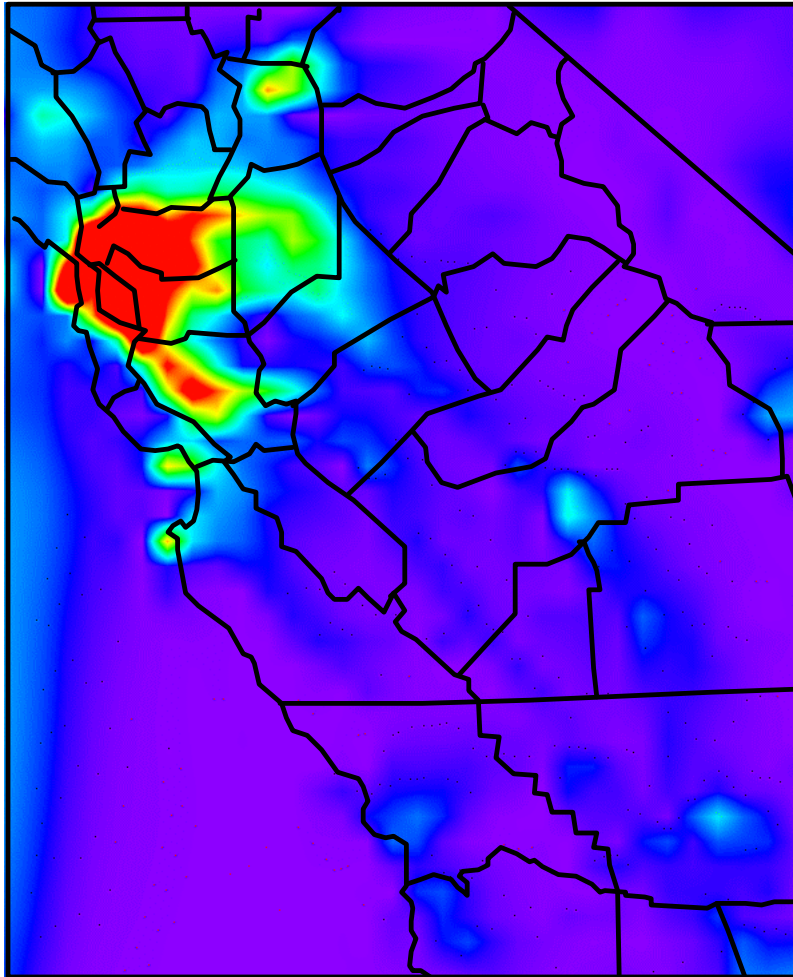


Figure 3.3-6. Plot of formaldehyde concentrations at midnight after two simulated days. Note that the western boundary has around 5 ppb of HCHO. These high HCHO concentrations appear to be due to transport from the model's boundary.



HCHO ppb

Figure 3.3-7. Plot of NO concentrations at 1:00 PM on the second simulated day. Note that the western boundary has over 0.5 ppb of NO. These moderate NO concentrations for over the ocean appear to be due to transport from the model's boundary.



NO ppb

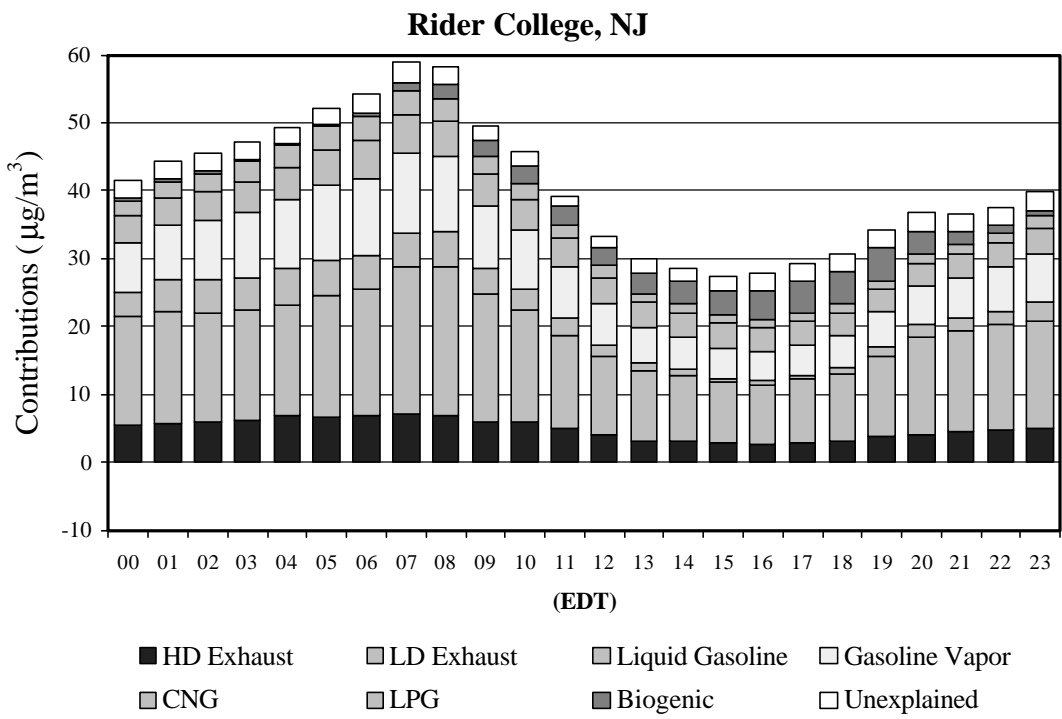


Figure 3.5-1. Average source contribution estimates of ambient hydrocarbons at Rider College, NJ during summer, 1995 by time of day. Source: Fujita and Lu, 1998.

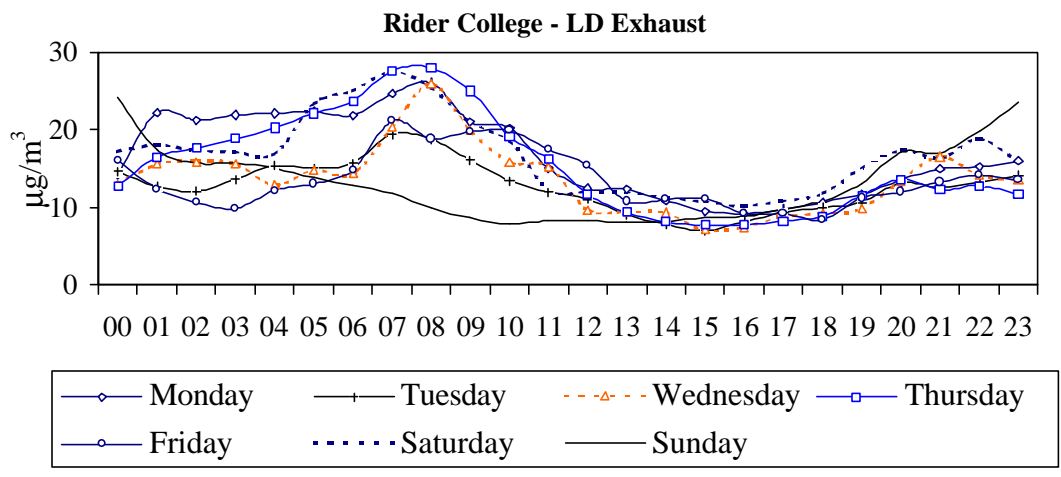


Figure 3.5-2. Average source contribution estimates of hydrocarbons at Rider College, NJ during summer, 1995 (EDT) by day of the week. Source: Fujita and Lu, 1998.

